Geophysical Research Letters

RESEARCH LETTER
10.1029/2024GL114397

An Empirical Parameterization to Separate Coarse and Fine Mode Aerosol Optical Depth Over Land

Xiaohan Li[1] **and Paul Ginoux**[2]

[1]Atmospheric and Oceanic Sciences Program, Princeton University, Princeton, NJ, USA, [2]NOAA Geophysical Fluid Dynamics Laboratory, Princeton, NJ, USA

Key Points:

- A parameterization linking the fine-mode fraction of aerosol optical depth to the Angstrom exponent was developed using AERONET data
- Validation of this parameterization with independent in situ nephelometer measurements demonstrates strong predictive capability
- Applying this parameterization to MODIS satellite data improves the predictive accuracy for fine- and coarse-mode aerosol optical depth

Supporting Information:

Supporting Information may be found in the online version of this article.

Correspondence to:

X. Li,
xiaohanl@princeton.edu

Citation:

Li, X., & Ginoux, P. (2025). An empirical parameterization to separate coarse and fine mode aerosol optical depth over land. *Geophysical Research Letters*, *52*, e2024GL114397. https://doi.org/10.1029/2024GL114397

Received 20 DEC 2024
Accepted 21 FEB 2025

Author Contributions:

Conceptualization: Xiaohan Li, Paul Ginoux
Data curation: Paul Ginoux
Investigation: Xiaohan Li
Methodology: Xiaohan Li
Supervision: Paul Ginoux
Validation: Xiaohan Li
Visualization: Xiaohan Li
Writing – original draft: Xiaohan Li
Writing – review & editing: Xiaohan Li, Paul Ginoux

Abstract Retrieving the fine-mode fraction (FMF) of aerosol optical depth from satellite data is crucial for understanding the impact of natural versus anthropogenic aerosols on climate and air quality. However, few high-quality global FMF products from MODIS exist. To address this gap, this study derives a new formulation of FMF as a function of the Ångström exponent (AE) based on over 20 years of AERONET measurements. Our results reveal a consistent FMF-AE relationship across continental regions, supporting the feasibility of globally estimating FMF through a simple empirical function based on AE. Validation with independent NOAA GML data sets shows predicted FMF errors mostly within 0.1. Finally, applying this parameterization to MODIS Aqua and Terra data significantly improved satellite-derived FMF agreement with AERONET compared to previous derivations. This parameterization provides a simple, valuable tool for accurately deriving FMF over land from MODIS and understanding its impact on climate and air quality.

Plain Language Summary Aerosols are liquid and solid particles suspended in the atmosphere, with sizes ranging from a few nanometers to tens of micrometers. These particles, produced by natural sources or human activities, play a significant role in air quality and climate. Estimating aerosol size distributions is important for understanding their climate and environmental impacts. However this remains challenging on regional and global scales due to the difficulties in retrieving this information from satellite observations. To address this, we created a parameterization that predicts the fraction of fine particles based on the measured spectral variation of light extinction by aerosols, known as the Ångström exponent (AE). By analyzing 20 years of ground-based sunphotometer data, we found a reliable pattern between AE and fine particle fraction. We then tested this method with in situ nephelometer data, and confirmed its accuracy. Finally, we applied our formula to satellite data, achieving better agreement with ground-based observations compared to previous parameterization efforts. Our formula can help scientists understand air pollution and its climate effects more accurately using satellite and ground-based data independently of location.

1. Introduction

Aerosols, solid or liquid particles suspended in the atmosphere, play a critical role in shaping the Earth's weather, air quality, and climate, yet remain one of the most uncertain aspects of climate science (Intergovernmental Panel on Climate Change, 2023). Based on their size, aerosols can be broadly classified into two categories: fine-mode and coarse-mode aerosols. Fine-mode aerosols, such as sulfate and carbonaceous aerosols, are typically smaller than 1 μm in diameter and are heavily influenced by anthropogenic emissions; in contrast, coarse-mode aerosols, such as mineral dust and sea salt aerosols, are typically larger than 1 μm and mechanically generated from natural sources (Ali et al., 2020; Ginoux et al., 2012; Yan, Zang, Zhao, & Husi, 2021).

Understanding the characteristics and distribution of fine- and coarse-mode aerosols is essential for distinguishing anthropogenic from natural aerosols and assessing their impacts on the Earth's climate systems. Aerosol optical depth (AOD), a widely used observable variable from ground-based and satellite observations, quantifies aerosol abundance and radiative influence by measuring the total extinction of light by aerosols along a vertical column of the atmosphere. A key parameter for separating fine- and coarse-mode contributions is the fine-mode fraction (FMF), which represents the proportion of fine particles in the total AOD. However, FMF derived from satellite-based AOD measurements is often unreliable, particularly over land, due to complexities in retrieval algorithms (Levy et al., 2013; Yan, Zang, Liang, et al., 2021). Similarly, satellite-derived aerosol optical properties, such as Ångström exponent retrievals, tend to be more accurate over oceans than over land, as the lower surface reflectance over water reduces uncertainties in the measured satellite signal (Levy et al., 2013). In comparison,

FMF derived from ground-based remote sensing data, such as the AErosol RObotic NETwork (AERONET) sun photometers that measure direct solar radiation and sky radiance (Holben et al., 1998, 2001), or in situ instruments (e.g., nephelometers, particle counters, and spectrophotometers) from the National Oceanic and Atmospheric Administration's Global Monitoring Laboratory (NOAA-GML), which directly measure aerosol size distributions and properties (Andrews et al., 2011, 2019), is more reliable. However, these ground-based observations are geographically limited and do not provide global coverage, making them insufficient for retrieving global aerosol size distributions.

The Ångström exponent (AE), which is the slope of the logarithm of AOD versus the logarithm of spectral light wavelength, is commonly used to characterize the wavelength dependence of AOD and to provide information on the aerosol size distribution (Eck et al., 1999). Taking advantage of the dependency of AE on aerosol size distribution, several studies have derived FMF from AE (Anderson et al., 2005; Eck et al., 2010; Koo et al., 2021; Pérez-Ramírez et al., 2015; Yan, Zang, Liang, et al., 2021; Yan, Zang, Zhao, & Husi, 2021). For example, using AERONET sunphotometer data during the ACE-Asia experiment, Anderson et al. (2005) showed that the submicron fraction (SMF) can be parameterized by a quadratic function of AE. This parameterization was later employed as an approximation of FMF and applied to MODIS satellite data by Pu and Ginoux (2016). Taking the co-function of FMF, the coarse fraction of AOD (i.e., COD) was derived (Pu & Ginoux, 2018) and was subsequently used in a series of dust studies on emission parameterization (Pu et al., 2020), prediction (Pu et al., 2019), assimilation for dust forecasting model (Di Tomaso et al., 2021), dust sources detection (Yu & Ginoux, 2022), field campaign (González-Romero et al., 2024), and satellite target mask (Green & Thompson, 2020), among others. Similarly, Pérez-Ramírez et al. (2015) reported a linear relationship between FMF and AE using AERONET data from five measurement sites. However, despite these efforts, existing parameterizations are often limited by the small number of observations and different functional forms across studies, raising concerns about their applicability to global satellite data (Anderson et al., 2005; Koo et al., 2021; Pérez-Ramírez et al., 2015). Complicating this further, AE are commonly observed to decrease as fine-mode aerosols grow, sometimes leading to negative correlations of FMF-AE at high FMF values (Eck et al., 2010, 2012). Such irregular patterns, possibly caused by aerosol aging or hygroscopic growth under humid conditions (Knight et al., 2024; Konovalov et al., 2021; Li & Bourg, 2019, 2024), are not captured in existing parameterizations. Therefore, it is crucial to employ more comprehensive data sets on regional and global scales to assess the presence of FMF-AE relationships and, if present, to establish reliable parameterizations.

To address the aforementioned knowledge gaps, we compiled 20 years of AERONET sunphotometer data across the globe to analyze patterns and generality of the relationship between FMF and AE over land. Based on these observations, we developed a parameterization of this relationship at both global and regional scales. The parameterization was then validated using independent data sets from in situ measurements from the NOAA-GML Federated Aerosol Network to ensure its robustness. Finally, we applied our parameterization to 20 years of satellite data from the Moderate Resolution Imaging Spectroradiometer Deep Blue (MODIS-DB) to extract fine-mode and coarse-mode aerosol information. Our parameterization demonstrates strong performance in capturing FMF and coarse-mode aerosol properties, outperforming other recent efforts due to its better accuracy, simple functional form and ease of application. This approach offers a valuable tool for enhancing global-scale analyses of dust and other aerosols, providing improved insights into aerosol distribution and behavior.

2. Data and Method

2.1. Data Set Description

This study employed three primary aerosol optical property data sets: (a) ground-based remote sensing data from AERONET, (b) surface in situ aerosol optical properties collected from field sites globally through NOAA GML Federated Aerosol Network of nephelometer, and (c) satellite observations from NASA's MODIS-DB aerosol products.

Specifically, the parameterizations developed in this study were based on 20 years of AERONET Version 3 direct sunphotometer measurements (Giles et al., 2019; Holben et al., 1998; Sinyuk et al., 2020). We used the aerosol optical properties for the total, fine and coarse mode aerosols using the spectral deconvolution algorithm (SDA) products (Level 1.5) at 500 nm wavelength (O'neill et al., 2003). We selected data points to ensure proper collocation with MODIS-DB Collection 6.1 data (N.Hsu et al., 2013; A. M. Sayer et al., 2019) collected from the Terra satellite (MOD) and the Aqua satellite (MYD), following the procedure outlined by Pu et al. (2020). Briefly,

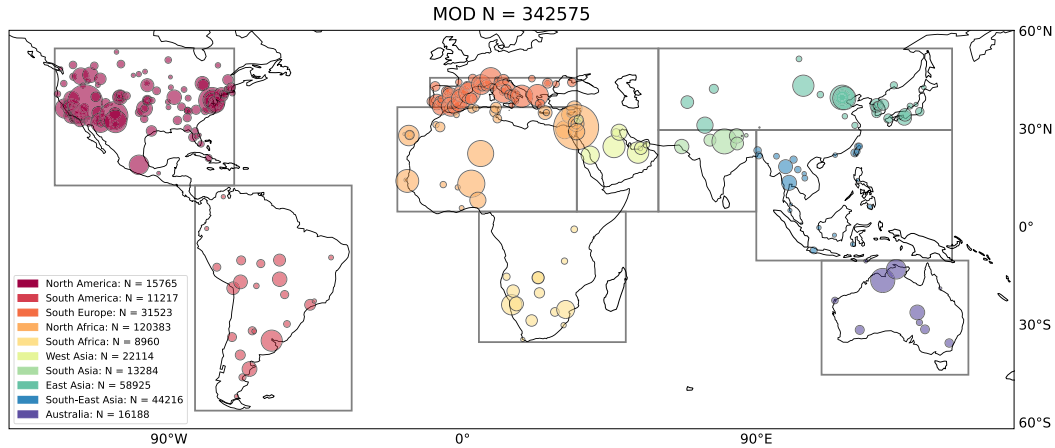

Figure 1. Geographical distribution of AERONET sites and co-located data of AERONET with MODIS-DB QA = 1 for Terra (MOD) from 2000 to 2022. The center and size of the colored circles represent the locations and the number of collocated data at each AERONET station. The colors correspond to different continental regions defined in Section 2.2. The total number of data points in each region is indicated in the legend.

AERONET data were averaged within a 1-hr window (±30 min) around the satellite overpass and within 10 km of AERONET site. These AERONET data sets formed the basis for the parameterization process and were subsequently used for comparison with MODIS data centered at the AERONET site. The number of collocated AERONET data points used in the parameterization and comparison processes was 342,575 for MOD and 324,649 for MYD. For simplicity, the terms "MYD data set" and "MOD data set" will henceforth refer to the AERONET data collocated with the MYD and MOD satellites, respectively. The geographical distribution of the MOD (for the period of 2000–2022) and MYD (for the period of 2003–2022) data sets are presented in Figure 1 and Figure S1 in Supporting Information S1.

To assess our formulation with independent measurements, we tested it against data from 8 sites included in the network of nephelometer instruments operated by NOAA-GML spanning 12 years for the period of 1996–2007 (Andrews et al., 2011). Aerosol light scattering and absorption coefficient were measured at 3 wavelengths (450, 550, and 700 nm) and for two particle size cuts. One for fine particles with aerodynamic diameter less than 1 μm, and the other for particles less than 10 μm. These instruments were operated under dry conditions, with RH-induced variations minimized by maintaining a low sample stream RH of 10%–40%, achieved through modest heating of 0–10°C (Anderson & Ogren, 1998). The selected parameters for validation were aerosol extinction at 550 nm and the AE calculated from the 450/550 nm wavelength pair, as both are closer to 500 nm, making them more comparable to the optical properties reported by AERONET at 500 nm. The sites included Bondville (BND, 40.05°N, 88.37°W), Heselbach (FKB, 48.54°N, 8.40°E), Mauna Loa (MLO, 19.54°N, 155.58°W), Niamey (NIM, 13.48°N, 2.18°E), Pt. Reyes (PYE, 38.09°N, −122.96°W), Southern Great Plains (SGP, 36.61°N, 97.49°W), Trinidad Head (THD, 41.05°N, 124.15°W), and Sable Island (WSA, 43.93°N, 60.01°W) (Andrews et al., 2011, 2019; Schmeisser et al., 2017).

Finally, our parameterization was applied to aerosol products retrieved daily from two polar-orbiting MODIS satellite instruments. These products include spectral AOD based on the Deep Blue algorithm (N. C. Hsu et al., 2006). Specifically, we used spectral AOD at 550 nm and the AE at 412/470 nm or 470/650 nm, depending on the AOD and the underlying surface, from Collection 6.1 Level 2 data (Levy et al., 2013; A. M. Sayer et al., 2019). The Level 2 data consist of geolocated granules of 10 × 10 pixels, each with a 1 km resolution at nadir. Only quality-assured (QA = 1) data were selected for analysis. Fine- and coarse-mode optical depths over land were derived at a 10 km resolution. The analysis was conducted for the Terra (2000–2022) and Aqua (2003–2022) satellites. The evaluation of our parameterization was performed by comparing collocated MODIS-DB data with AERONET observations.

We note that AE can vary significantly depending on the wavelength range over which it is computed and, consequently, its sensitivity to aerosol size may also change with wavelength (Eck et al., 1999; Reid et al., 1999). Therefore, the choice of the wavelength band for the FMF-AE relationship should be carefully considered. As

discussed above, this study primarily focuses on the FMF-AE relationship around 500 nm, as the parameterization is based on AE and FMF at 500 nm from AERONET SDA retrievals.

2.2. Study Regions

To examine the FMF-AE relationship across different geographical areas, we divided the globe into 10 continental regions as follows: (a) North America (125°W, 70°W, 13°N, 55°N); (b) South America (82°W, 34°W, 56°S, 13°N); (c) South Europe (10°W, 35°E, 37°N, 46°N); (d) North Africa (20°W, 35°E, 5°N, 37°N); (e) South Africa (5°E, 50°E, 35°S, 5°N); (f) West Asia (35°E, 60°E, 5°N, 55°N); (g) South Asia (60°E, 90°E, 5°N, 30°N); (h) East Asia (60°E, 150°E, 30°N, 55°N); (i) South-East Asia (90°E, 150°E, 10°S, 30°N); and (j) Australia (110°E, 155°E, 45°S, 10°S). These regions are depicted with different bounding boxes in Figure 1.

2.3. Parameterization Procedures

By definition, at a given wavelength λ, the AE (denoted as α) is defined as

$$\alpha = -\frac{d \ln \tau_a}{d \ln \lambda} \tag{1}$$

where τ_a is the total AOD. If we assume the presence of two aerosol modes, then

$$\tau_a = \tau_c + \tau_f \tag{2}$$

where τ_c and τ_f are the coarse-mode and fine-mode optical depths, respectively. By combining Equations 1 and 2, it is mathematically rigorous to show that (see Text S1 in Supporting Information S1 for derivation)

$$\alpha = \eta\alpha_f + (1-\eta)\alpha_c \tag{3}$$

where $\eta = \tau_f/\tau_a$ is the FMF of aerosol optical depth, and α_f and α_c are the fine-mode and coarse-mode AE, respectively.

The objective of this study is to develop an empirical parameterization, which separates the contribution of fine-mode and coarse-mode aerosols to the AOD. In other words, we aim to derive an empirical equation for η as a function of α, that is, $\eta = f(\alpha)$, where f is the function to be determined. As shown in Figure 2a for the AERONET MOD data set (see Figure S2 in Supporting Information S1 for MYD data set), a consistent trend between AERONET-derived FMF and AE is observed across all 10 studied continental regions. This global consistency strongly suggests that it is feasible to estimate the contribution of coarse-mode and fine-mode aerosols based on α using a single, simple empirical function applicable on a global scale.

As derived from Equation 3, two constraints are necessary for the FMF-AE parameterization to be effective: (a) when $\eta = 1$, $\alpha = \alpha_f$, and (b) when $\eta = 0$, $\alpha = \alpha_c$. In our analysis of AERONET data at a wavelength of 500 nm, we find that α_c values are consistent across the 10 regions for both the MOD and MYD data sets, with small variations ranging from -0.150 to -0.153 across different continental regions, and a global mean of -0.15 ± 0.01 (see Figure S3 and Table S1 in Supporting Information S1 for details). In contrast, α_f exhibits significantly greater variability across regions and between the two data sets, likely due to differences in aerosol types, aerosol aging, and hygroscopic growth. For MOD, α_f ranges from 1.40 to 1.80 across 10 continental regions, with a global mean of 1.50 ± 0.34, while for MYD, α_f varies from 1.40 to 1.87 across 10 continental regions, with a global mean of 1.52 ± 0.34 (see Figure S4 and Table S2 in Supporting Information S1 for details). We note that these AE values represent regional mean values from the AERONET SDA products at 500 nm. However, individual AE values can fall outside this range. For example, previous studies have reported that aged smoke transported from California has resulted in low AE values in fine-mode aerosols, as low as 0.67 (Eck et al., 2023). Our analysis shows that the α_c value of -0.15 and the α_f value of approximately 1.5 are consistent with previous studies (Eck et al., 2010; O'Neill et al., 2001). To account for the fluctuations of α_c and α_f, in developing our empirical parameterization for different regions, we applied the following constraints: when $\eta = 0$ or $\eta = 1$, α must fall within one standard deviation of the regional mean of α_c and α_f, respectively.

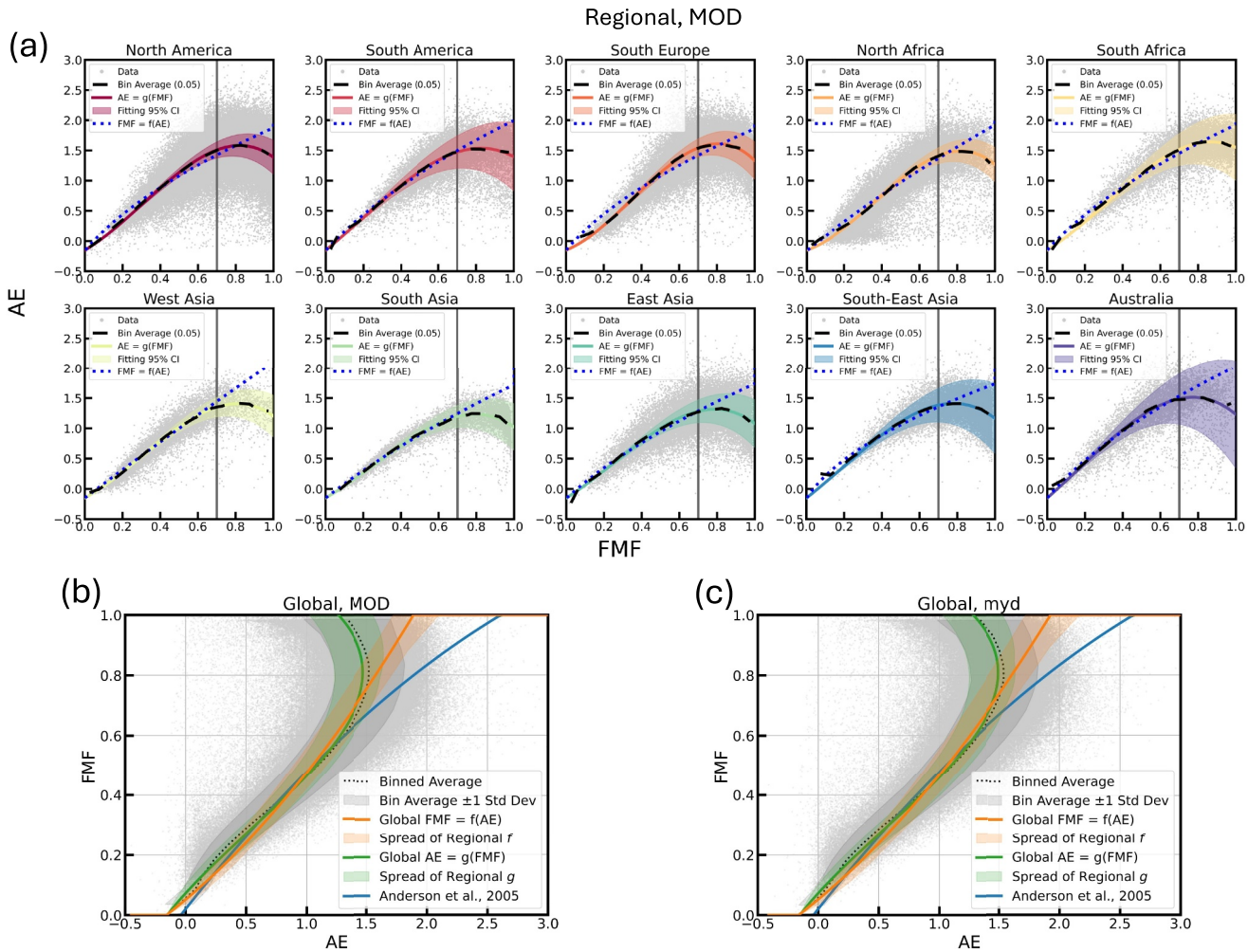

Figure 2. (a) AE versus FMF across different regions for the AERONET MOD data set from SDA retrieval at 500 nm wavelength. The gray dots represent individual AERONET data points, while the dashed black lines indicate the binned average of AERONET data, with bins grouped by FMF in increments of 0.05. The shaded colored areas and corresponding solid lines in the center represent the 95% confidence interval (CI) and the best-fit function for AE = g(FMF). The blue dotted line represents the best-fit function where FMF is expressed as a function of AE, that is, FMF = f(AE). (b) FMF versus AE at the global scale for the MOD data set. Gray dots represent individual AERONET data points. The black dashed line indicates the binned average, with data binned by FMF in increments of 0.05, and the shaded gray area represents the range of the binned average ±1 standard deviation. The orange solid line depicts the global relationship FMF = f(AE), with the shaded orange area showing the variability of regional f. Similarly, the green solid line represents the global relationship AE = g(FMF), with the shaded green area indicating the variability of regional g. The blue solid line corresponds to the prediction by Anderson et al. (2005). (c) FMF versus AE at the global scale for the MYD data set, with symbols and shading meaning the same as in (b).

Regarding the choice of functional form, we tested several options—including linear, second- and third-order polynomials, sigmoid, exponential functions—based on trends observed in the data. As will be presented in the Results and Discussion section, the third-order and second-order polynomial provided the best fit. We note that while aerosols are commonly grouped into two modes, a middle mode has also been observed under certain conditions, such as cloud-processed aerosols (Eck et al., 2012) and dust aerosols influenced by atmospheric processing (Gianelli et al., 2013). The presence of three aerosol modes may introduce inherent uncertainties in current parameterizations that assume only two aerosol modes.

2.4. Comparison of AERONET and MODIS Deep Blue Data

To compare MODIS-DB AOD data at a 550 nm wavelength with AERONET AOD data measured at 500 nm, it is necessary to convert the AERONET AOD values to 550 nm. This conversion is performed using the following equation:

$$\mathrm{AOD}_{550} = \mathrm{AOD}_{500} \times \left(\frac{550}{500}\right)^{-\alpha} \quad (4)$$

where α is the AE derived from AERONET data at 500 nm wavelength. Applying this conversion ensures consistency between the accurate comparison of AOD, fine-mode optical depth (FOD) and coarse-mode optical depth (COD) values at 550 nm between MODIS and AERONET data as in Section 3.3. We acknowledge that a second-order fit of AOD versus wavelength in logarithmic coordinates can provide a more accurate interpolation (Eck et al., 1999; A. M. Sayer et al., 2019). However, for consistency with previous AERONET versus MODIS-DB validation studies and computational efficiency, we use a first-order extrapolation, as the uncertainty introduced by the differences in interpolation/extrapolation schemes is minimal compared to the overall data variability in different continental regions.

3. Results

3.1. Relationship Between AE and FMF From AERONET Data Set

The black-dashed lines in Figure 2a and Figure S2 in Supporting Information S1 show the center line of the AERONET data, binned and averaged with FMF, with a bin size of 0.05. From these center lines, a consistent pattern is evident in the relationship between AE and FMF across all continental regions in both the AERONET MYD and MOD data sets. Specifically, when FMF < 0.7, FMF increases monotonically with AE. However, when FMF exceeds approximately 0.7 and AE falls within the range of 1.0–1.5, a reversal in AE values is observed. This negative correlation, where AE decreases as FMF increases at high FMF, has also been noted in previous studies and is likely attributed to factors such as aerosol aging or hygroscopic growth (Eck et al., 2010, 2012).

The reversal of AE with increasing FMF suggests that expressing AE as a function of FMF, that is, AE = g(FMF), may provide a better strategy for characterizing the data than FMF = f(AE). Notably, an AE value greater than 1.0 can correspond to multiple FMF values, whereas the inverse relationship does not exhibit this ambiguity. Therefore, we modeled AE = g(FMF) using a third-order polynomial fit across different regions, given by $\alpha = p + q\eta + r\eta^2 + s\eta^3$, where p, q, r, and s are fitting parameters to be determined according to the constraints discussed in Section 2.3. The best-fit function g for MOD data set in each continental region is shown by the solid colored lines in the subplots of Figure 2a (see Figure S2 in Supporting Information S1 for results of MYD data set), with the shaded regions representing the 95% confidence interval (CI) for the fit. Our results indicate that the fit for g is highly accurate, with the fitted curve nearly overlapping with the binned average center line of the data, effectively capturing the central behavior of the data. The fitted parameters p, q, r, and s for different regions are listed in Table S3 in Supporting Information S1. At the global scale, the function g is shown by the solid green lines in Figures 2b and 2c and can be represented as:

$$\alpha = g(\eta) = \begin{cases} -3.205\,\eta^3 + 2.706\,\eta^2 + 1.913\,\eta - 0.151, & \text{for MOD} \\ -3.310\,\eta^3 + 2.836\,\eta^2 + 1.905\,\eta - 0.151, & \text{for MYD} \end{cases} \quad (5)$$

However, for practical applications, modeling FMF = f(AE) is preferred over AE = g(FMF), as AE is a directly measurable property, whereas FMF is typically a derived or predicted variable. To address this requirement, and based on observations that AE inversion occurs when FMF > 0.7, along with the uncertainties of FMF > 0.7 being too large to provide meaningful information about the dependence of AE on FMF, we restricted the data set to include only data points where FMF < 0.7 for constructing the relationship FMF = f(AE). Regarding this truncation, we emphasize that the primary motivation and application of this study is to determine dust COD. Thus, restricting the analysis to FMF < 0.7 is justified, as this approach more effectively isolates the coarse-mode dust component. After applying this data filter, we determined that a quadratic function outperformed both exponential and third-order polynomial functions in capturing the relationship between AE and FMF. The function f is defined as $\eta = a + b\alpha + c\alpha^2$, with the constraints outlined in Section 2.3. The best-fit results for different regions are shown as dotted blue lines in Figure 2a for MOD data set (see Figure S2 in Supporting Information S1 for MYD data set). The dotted blue line effectively represents the relationship between AE and FMF, aligning closely with g (i.e., AE = g(FMF)) for AE values below 1.0 across all regions, although

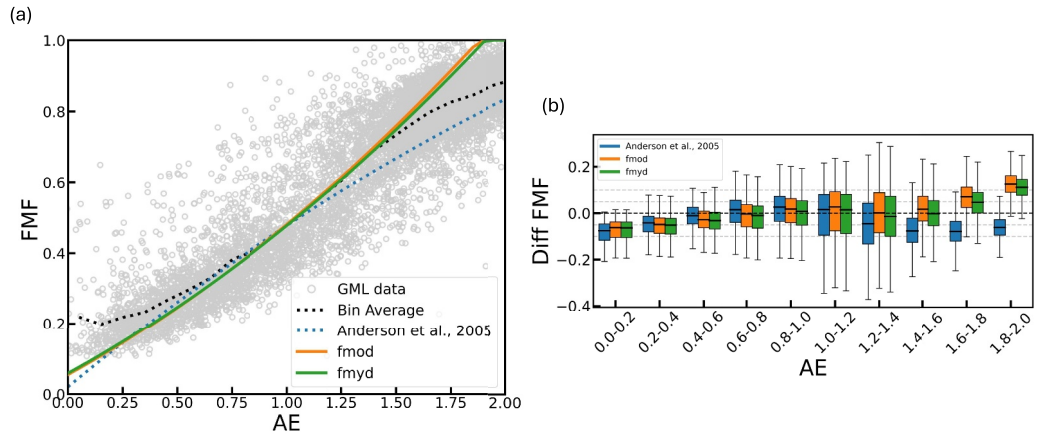

Figure 3. (a) FMF versus AE. The gray dots represent data from the NOAA-GML data set across eight measurement sites. The black dotted line indicates the binned average, with data binned by AE in increments of 0.1. The orange and green solid lines illustrate the predicted relationships by f for MOD (f_{mod}) and MYD (f_{myd}), respectively. The blue dashed lines represent the predicted relationships from Anderson et al. (2005). (b) Box plot showing the difference between predicted FMF and actual FMF (Diff FMF) across different AE bins for NOAA-GML data set. The blue, orange and green labels correspond to the results from Anderson, f_{mod}, and f_{myd}, respectively.

large and significant deviations are observed at higher FMF values. Overall, most of the predictions from f remain within the 95% CI of g, demonstrating its robustness and reliability.

The fitted parameters a, b, and c for different regions are listed in Table S4 in Supporting Information S1. At the global scale, the function $f(\alpha)$ is represented by the solid orange lines in Figures 2b and 2c for MOD and MYD respectively and is expressed as:

$$\eta = f(\alpha) = \begin{cases} 0.087\ \alpha^2 + 0.338\ \alpha + 0.051, & \text{for MOD} \\ 0.082\ \alpha^2 + 0.333\ \alpha + 0.052, & \text{for MYD} \end{cases} \tag{6}$$

For the convenience of discussion, we refer to $f(\alpha)$ for MOD and MYD as f_{mod} and f_{myd}, respectively, hereafter. As shown in Figure 3a, the difference between the predictions of f_{mod} and f_{myd} is minimal and can be considered negligible. Therefore, we averaged f_{mod} and f_{myd} to obtain f_{mean}, which serves as the standardized parameterization:

$$\eta = f_{\mathrm{mean}}(\alpha) = 0.085\ \alpha^2 + 0.336\ \alpha + 0.051 \tag{7}$$

Again, we note that the parameterization from Equations 6 and 7 is fitted only to the FMF < 0.7 data. Since the primary purpose of this study is to better identify coarse-mode aerosols, such as dust, this justification and application are well-founded for this purpose.

3.2. Validation of Parameterization With NOAA-GML Data

The gray dots in Figure 3a depict the relationship between SMF and AE derived from the NOAA-GML data set across eight measurement sites, with filtration of the scattering coefficient larger than 5 Mm^{-1} for valid values (Andrews et al., 2019; Schmeisser et al., 2017). It is notable that systematic differences exist between SMF and FMF depending on the truncation schemes employed (Anderson et al., 2005; O'Neill et al., 2023). However, for the purposes of this analysis, we temporarily neglect these differences to focus on comparing the trend of the FMF-AE relationship predicted by our parameterization, which is based on AERONET FMF, with the SMF-AE relationship observed in the NOAA-GML data set. Unlike the AERONET data, the NOAA-GML data set does not exhibit a distinct reversal of AE to lower values as SMF approaches 1. This discrepancy may be attributed to dry and ambient humidity conditions for NOAA-GML nephelometer and AERONET sunphotometer, respectively (Andrews et al., 2019; Holben et al., 1998).

Despite these significant differences between the AERONET and NOAA-GML data sets, our parameterization based on AERONET data successfully captures the relationship between AE and SMF in the NOAA-GML data set, particularly when AE < 1.6. The functions f for MOD (f_{mod}) and MYD (f_{myd}) yield comparable or even lower root mean square errors (RMSE) than the predictions from Anderson et al. (2005), which is a parameterization for SMF and AE, as shown in the box plot of the difference in FMF in Figure 3b. However, due to the inherent differences in the data sets, when AE > 1.6, f_{mod} and f_{myd} tend to overestimate NOAA-GML SMF by approximately 0.1. For comparison, Anderson's parameterization tends to underestimate FMF by approximately ∼0.06. This analysis demonstrates the applicability of our parameterization, particularly when AE values are low. Specifically, when AE < 1.6, our predictions slightly outperform those of Anderson et al. (2005).

We note that there are inherent differences between the NOAA-GML data set, which represents surface-based nephelometer measurements under dry aerosol conditions, and the AERONET data set, which represents total column retrievals under ambient conditions. The eight NOAA sites with nephelometers generally exhibit low fine-mode AOD levels. Additionally, since these measurements are taken under dried (rather than ambient) aerosol conditions, fine-mode aerosols at lower concentrations (lower AODs) experience reduced coagulation and condensation rates. As a result, these aerosols tend to be smaller, less aged, and/or less humidified compared to the ambient aerosol observed in AERONET data. However, we include this comparison to provide an independent evaluation of the parameterization. Notably, despite these differences, the FMF-AE parameterization derived from AERONET exhibits reasonable agreement with the NOAA nephelometer data set, suggesting that the relationship remains applicable to surface-based observations under dry conditions. This consistency indicates that the parameterization captures fundamental aerosol optical properties that are not entirely dependent on measurement conditions, reinforcing its robustness.

Finally, we note that the determination of the coefficients a, b, and c in the function f in Equation 6 is sensitive to the constraints applied on α_c and α_f. Currently, we present the results of f with a 1 standard deviation constraint on α_c and α_f. When a 2 standard deviation constraint is allowed for α_c and α_f, the fitting results align better with the GML data at higher AE values (see Figure S5 in Supporting Information S1 for details). However, this 2 standard deviation constraint does not improve MODIS satellite retrievals, as the AE values for MODIS satellites are typically constrained to be less than 1.8. There is a systematic mismatch between the AE values for GML, AERONET, and the satellite data. Given these uncertainties, we choose the current f functions (i.e., Equation 6) for satellite data analysis, and we emphasize the need for more accurate satellite data AE measurements.

3.3. Partitioning Fine and Coarse Modes From MODIS Data

Figure 4 presents the comparison between MODIS-DB QA = 1 and AERONET data for the MOD data set with AOD > 0.05 to minimize the impact of retrieval uncertainties (see Figure S6 in Supporting Information S1 for the MYD data set) (Levy et al., 2013; A. M. Sayer et al., 2013). Figure 4a shows the comparison between MODIS AOD and AERONET AOD, demonstrating good agreement with a correlation of 0.86 and a mean bias of 0.15. Similarly, the comparison between MODIS-derived FOD based on f_{mod} and AERONET FOD also shows strong agreement, with a correlation of 0.82 and a mean bias of 0.15.

To evaluate the parameterization from this study in comparison to previous parameterizations, Figures 4c and 4d present box plots of the differences between predictions and actual values for FOD and COD. These are based on Anderson's parameterization, the f_{mod} and f_{mean} parameterization developed in this study, as a function of AERONET FOD. In general, the f_{mod} and f_{mean} parameterization predicts both FOD and COD more accurately than Anderson's parameterization, with smaller deviations from AERONET data for both variables.

However, it is important to recognize the inherent limitations and systematic differences between the AERONET and MODIS data sets due to their retrieval algorithms. As expected from the information content of sensors and algorithms (Levy et al., 2010; A. M. Sayer et al., 2012, 2013; Wagner & Silva, 2008), significant scatter is observed in MODIS-DB when compared to AERONET with respect to the AE. Further complicating the comparison, the MODIS-DB algorithm introduces constraints to manage retrieval limitations and avoid unphysical values. Specifically, Deep Blue limits AE to $0 \leq \mathrm{AE} \leq 1.8$, fixes AE at 1.5 over vegetated surfaces under low-AOD conditions, and restricts AE to ≤1 over bright surfaces (N. Hsu et al., 2013). These constraints can result in artifacts, particularly under low-AOD conditions, further complicating the retrieval of aerosol-related quantities beyond AOD. As emphasized by previous work (Hasekamp & Landgraf, 2007; Kokhanovsky et al., 2010),

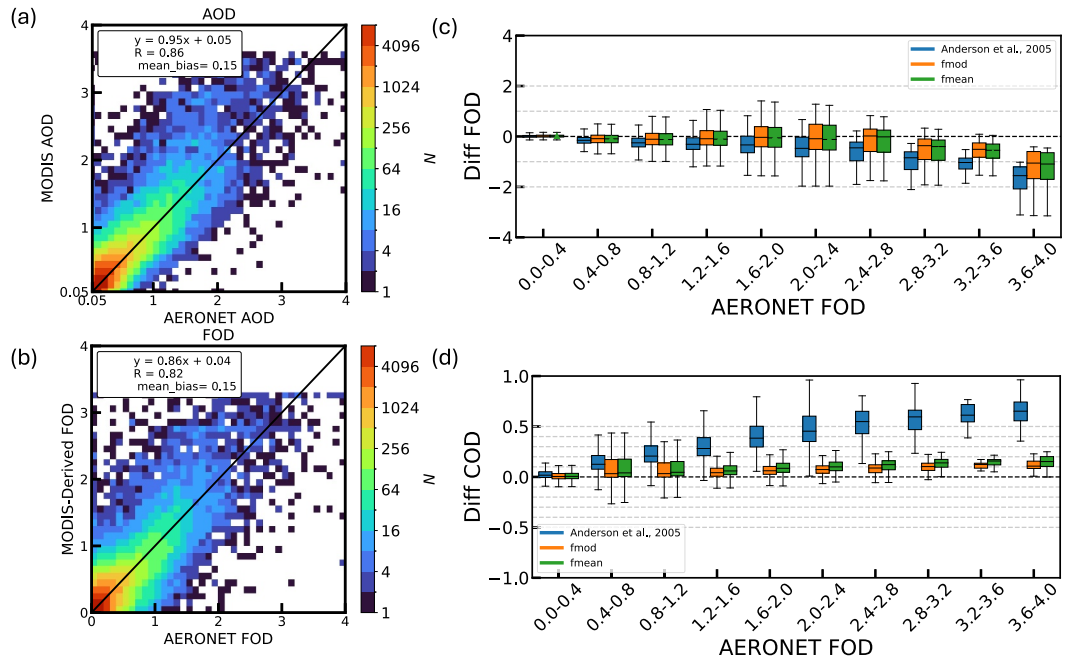

Figure 4. Density histograms of (a) MODIS-DB AOD versus AERONET AOD and (b) MODIS-Derived FOD versus AERONET FOD at 550 nm for the MOD data set. The colorbar represents the density of values in each grid cell binned in intervals of 0.1. Box plots of the differences between (c) MODIS-Derived FOD and AERONET FOD (Diff FOD), and (d) MODIS-Derived COD and AERONET COD (Diff COD) versus AERONET FOD at 550 nm. The blue, orange, and green boxes indicate results from Anderson et al. (2005), f_{mod}, and f_{mean}, respectively.

reliable inference of aerosol parameters like AE over land requires multiangular or polarimetric measurements, particularly in low-AOD conditions. These systematic differences between AERONET and MODIS data sets underscore the importance of carefully considering retrieval algorithms when analyzing aerosol properties.

Despite these limitations, our parameterization significantly improves COD predictions compared to Anderson's parameterization. Notably, for COD predictions, Anderson's formula systematically overestimates COD, especially in high-FOD regions, with overestimations exceeding 0.5. In contrast, our new formulation significantly reduces this positive bias, limiting it to approximately 0.1. This finding indicates that previous studies applying Anderson's parameterization to partition FOD and COD may overestimate COD in polluted regions by approximately 20%, highlighting the need to revisit these estimates using our new parameterization (Pu et al., 2022; Pu & Ginoux, 2016; Yu & Ginoux, 2022).

4. Conclusion and Discussion

Previous studies partitioning the satellite AOD between fine and coarse modes have often applied the parameterization proposed by Anderson et al. (2005) based on AERONET sunphotometers data. Since then, the volume of AERONET data has considerably increased, as well as the quality of the data with the recently released version 3. It was therefore tempting to revisit their formulation, and eventually provide a better fit with AERONET and independent data sets.

We reformulate the dependency of FMF and AE using 20 years of AERONET SDA data, both globally and regionally, to investigate the relationship between FMF and AE at different scales over land. Our results reveal a consistent trend between FMF and AE at both global and regional scales, supporting the feasibility of developing a reliable parameterization. This parameterization was further validated against the NOAA-GML data set, showing good agreement with observed results.

When applied to MODIS data, our new parameterization demonstrates high accuracy in capturing FOD and COD signals across both pristine and highly polluted regions, outperforming the commonly used Anderson parameterization. Specifically, our analysis reveals that previous dust studies utilizing Anderson's parameterization tend

to overestimate dust COD by approximately 20% and overestimate COD in highly polluted regions by more than 0.6. These findings highlight the need to revisit and refine conclusions from prior studies on dust aerosols using our updated parameterization to improve accuracy and reliability in understanding global aerosol dynamics.

We note that our parameterization is derived from AERONET and validated using the NOAA-GML data set, both of which are independent of any satellite platform. This suggests that the parameterization could potentially be applicable to other satellite instruments on SUOMI-NPP (A. Sayer et al., 2018) and NOAA20 (Lee et al., 2024). Therefore, future studies would be valuable in further assessing its applicability by explicitly comparing its accuracy against TROPOMI (Chen et al., 2024) and PARASOL (L. Li et al., 2020) retrieved fine- and coarse-mode AOD using GRASP-algorithm (Lopatin et al., 2021).

Data Availability Statement

The NOAA-GML data set used in this study is publicly available and can be downloaded from the NOAA-GML aerosol FTP server at https://gml.noaa.gov/aftp/aerosol/. Additional information about NOAA-GML and its instrumentation can be accessed at https://gml.noaa.gov/aero/instrumentation/instrum.html. AERONET direct sun measurements are available at the AERONET Aerosol Data website https://aeronet.gsfc.nasa.gov/new_web/aerosols.html. This study used Version 3 data, specifically Level 1.5 quality assurance. While Level 2 data were manually inspected in the past, the current process is automated and may include issues with false screening. The MODIS aerosol products used in this study are MOD04_L2 for Terra and MYD04_L2 for Aqua, available in the NASA MODIS repository (Levy et al., 2015a, 2015b). Additional information about NASA Deep Blue aerosol project, including further documentation and links, can befound online at https://earth.gsfc.nasa.gov/climate/data/deep-blue.

Acknowledgments
This research was supported by the National Oceanic and Atmospheric Administration, U.S. Department of Commerce under Award NA23OAR4320198. The statements, findings, conclusions, and recommendations are those of the author(s) and do not necessarily reflect the views of the National Oceanic and Atmospheric Administration, or the U.S. Department of Commerce. The authors would like to thank John Dunne and Ryan Kramer for the internal review and very helpful suggestions, and Yan Yu at Peking University for helpful discussions.

References

Ali, M. A., Nichol, J. E., Bilal, M., Qiu, Z., Mazhar, U., Wahiduzzaman, M., et al. (2020). Classification of aerosols over Saudi Arabia from 2004–2016. *Atmospheric Environment*, *241*, 117785. https://doi.org/10.1016/j.atmosenv.2020.117785

Anderson, T. L., & Ogren, J. A. (1998). Determining aerosol radiative properties using the TSI 3563 integrating nephelometer. *Aerosol Science and Technology*, *29*(1), 57–69. https://doi.org/10.1080/02786829808965551

Anderson, T. L., Wu, Y., Chu, D. A., Schmid, B., Redemann, J., & Dubovik, O. (2005). Testing the MODIS satellite retrieval of aerosol fine-mode fraction. *Journal of Geophysical Research*, *110*(D18), D18204. https://doi.org/10.1029/2005jd005978

Andrews, E., Ogren, J., Bonasoni, P., Marinoni, A., Cuevas, E., Rodríguez, S., et al. (2011). Climatology of aerosol radiative properties in the free troposphere. *Atmospheric Research*, *102*(4), 365–393. https://doi.org/10.1016/j.atmosres.2011.08.017

Andrews, E., Sheridan, P. J., Ogren, J. A., Hageman, D., Jefferson, A., Wendell, J., et al. (2019). Overview of the NOAA/ESRL federated aerosol network. *Bulletin of the American Meteorological Society*, *100*(1), 123–135. https://doi.org/10.1175/bams-d-17-0175.1

Chen, C., Litvinov, P., Dubovik, O., Fuertes, D., Matar, C., Miglietta, F., et al. (2024). Retrieval of aerosol and surface properties at high spatial resolution: Hybrid approach and demonstration using sentinel-5p/TROPOMI and PRISMA. *Journal of Geophysical Research: Atmospheres*, *129*(15), e2024JD041041. https://doi.org/10.1029/2024jd041041

Di Tomaso, E., Escribano, J., Basart, S., Ginoux, P., Macchia, F., Barnaba, F., et al. (2021). Monarch regional reanalysis of desert dust aerosols: An initial assessment. In *International technical meeting on air pollution modelling and its application* (pp. 241–247).

Eck, T. F., Holben, B., Reid, J., Dubovik, O., Smirnov, A., O'neill, N., et al. (1999). Wavelength dependence of the optical depth of biomass burning, urban, and desert dust aerosols. *Journal of Geophysical Research*, *104*(D24), 31333–31349.

Eck, T. F., Holben, B., Sinyuk, A., Pinker, R., Goloub, P., Chen, H., et al. (2010). Climatological aspects of the optical properties of fine/coarse mode aerosol mixtures. *Journal of Geophysical Research*, *115*(D19), D19205. https://doi.org/10.1029/2010jd014002

Eck, T. F., Holben, B. N., Reid, J., Giles, D., Rivas, M., Singh, R. P., et al. (2012). Fog-and cloud-induced aerosol modification observed by the Aerosol Robotic Network (AERONET). *Journal of Geophysical Research*, *117*(D7), D07206. https://doi.org/10.1029/2011jd016839

Eck, T. F., Holben, B. N., Reid, J. S., Sinyuk, A., Giles, D. M., Arola, A., et al. (2023). The extreme forest fires in California/Oregon in 2020: Aerosol optical and physical properties and comparisons of aged versus fresh smoke. *Atmospheric Environment*, *305*, 119798. https://doi.org/10.1016/j.atmosenv.2023.119798

Gianelli, S. M., Lacis, A. A., Carlson, B. E., & Hameed, S. (2013). Evidence of a weakly absorbing intermediate mode of aerosols in AERONET data from Saharan and Sahelian sites. *Journal of Geophysical Research: Atmospheres*, *118*(22), 12–661. https://doi.org/10.1002/2013jd020342

Giles, D. M., Sinyuk, A., Sorokin, M. G., Schafer, J. S., Smirnov, A., Slutsker, I., et al. (2019). Advancements in the aerosol robotic network (AERONET) version 3 database–automated near-real-time quality control algorithm with improved cloud screening for sun photometer aerosol optical depth (AOD) measurements. *Atmospheric Measurement Techniques*, *12*(1), 169–209. https://doi.org/10.5194/amt-12-169-2019

Ginoux, P., Prospero, J. M., Gill, T. E., Hsu, N. C., & Zhao, M. (2012). Global-scale attribution of anthropogenic and natural dust sources and their emission rates based on MODIS deep blue aerosol products. *Reviews of Geophysics*, *50*(3), RG3005. https://doi.org/10.1029/2012rg000388

González-Romero, A., González-Flórez, C., Panta, A., Yus-Díez, J., Córdoba, P., Alastuey, A., et al. (2024). Characterization of the particle size distribution, mineralogy, and Fe mode of occurrence of dust-emitting sediments from the Mojave desert, California, USA. *Atmospheric Chemistry and Physics*, *24*(16), 9155–9176. https://doi.org/10.5194/acp-24-9155-2024

Green, R. O., & Thompson, D. R. (2020). An Earth science imaging spectroscopy mission: The Earth surface mineral dust source investigation (EMIT). In *IGARSS 2020-2020 IEEE International Geoscience and Remote Sensing Symposium* (pp. 6262–6265).

Hasekamp, O. P., & Landgraf, J. (2007). Retrieval of aerosol properties over land surfaces: Capabilities of multiple-viewing-angle intensity and polarization measurements. *Applied Optics*, *46*(16), 3332–3344. https://doi.org/10.1364/ao.46.003332

Holben, B. N., Eck, T. F., Slutsker, I. a., Tanré, D., Buis, J., Setzer, A., et al. (1998). Aeronet—A federated instrument network and data archive for aerosol characterization. *Remote Sensing of Environment*, *66*(1), 1–16. https://doi.org/10.1016/s0034-4257(98)00031-5

Holben, B. N., Tanré, D., Smirnov, A., Eck, T., Slutsker, I., Abuhassan, N., et al. (2001). An emerging ground-based aerosol climatology: Aerosol optical depth from AERONET. *Journal of Geophysical Research*, *106*(D11), 12067–12097. https://doi.org/10.1029/2001jd900014

Hsu, N., Jeong, M.-J., Bettenhausen, C., Sayer, A., Hansell, R., Seftor, C., et al. (2013). Enhanced deep blue aerosol retrieval algorithm: The second generation. *Journal of Geophysical Research: Atmospheres*, *118*(16), 9296–9315. https://doi.org/10.1002/jgrd.50712

Hsu, N. C., Tsay, S.-C., King, M. D., & Herman, J. R. (2006). Deep blue retrievals of Asian aerosol properties during ACE-Asia. *IEEE Transactions on Geoscience and Remote Sensing*, *44*(11), 3180–3195. https://doi.org/10.1109/tgrs.2006.879540

Intergovernmental Panel on Climate Change. (2023). Climate change 2023: Synthesis report. Contribution of working groups I, II and III to the sixth assessment report of the intergovernmental panel on climate change. https://doi.org/10.59327/IPCC/AR6-9789291691647

Knight, J. W., Forsythe, J. E., Zhang, X., Rafferty, A., Orr-Ewing, A. J., & Cotterell, M. I. (2024). Wavelength-and ph-dependent optical properties of aqueous aerosol particles containing 4-nitrocatechol. *ACS Earth and Space Chemistry*, *8*(11), 2198–2208. https://doi.org/10.1021/acsearthspacechem.4c00179

Kokhanovsky, A. A., Budak, V. P., Cornet, C., Duan, M., Emde, C., Katsev, I. L., et al. (2010). Benchmark results in vector atmospheric radiative transfer. *Journal of Quantitative Spectroscopy and Radiative Transfer*, *111*(12–13), 1931–1946. https://doi.org/10.1016/j.jqsrt.2010.03.005

Konovalov, I. B., Golovushkin, N. A., Beekmann, M., & Andreae, M. O. (2021). Insights into the aging of biomass burning aerosol from satellite observations and 3D atmospheric modeling: Evolution of the aerosol optical properties in siberian wildfire plumes. *Atmospheric Chemistry and Physics*, *21*(1), 357–392. https://doi.org/10.5194/acp-21-357-2021

Koo, J.-H., Lee, J., Kim, J., Eck, T. F., Giles, D. M., Holben, B. N., et al. (2021). Investigation of the relationship between the fine mode fraction and Ångström exponent: Cases in Korea. *Atmospheric Research*, *248*, 105217. https://doi.org/10.1016/j.atmosres.2020.105217

Lee, J., Hsu, N. C., Kim, W. V., Sayer, A. M., & Tsay, S.-C. (2024). Viirs version 2 deep blue aerosol products. *Journal of Geophysical Research: Atmospheres*, *129*(6), e2023JD040082. https://doi.org/10.1029/2023jd040082

Levy, R., & Hsu, C. (2015a). MODIS atmosphere L2 aerosol product [Dataset]. *NASA MODIS Adaptive Processing System, Goddard Space Flight Center*. https://doi.org/10.5067/MODIS/MOD04_L2.061

Levy, R., & Hsu, C. (2015b). MODIS atmosphere L2 aerosol product [Dataset]. *NASA MODIS Adaptive Processing System, Goddard Space Flight Center*. https://doi.org/10.5067/MODIS/MYD04_L2.061

Levy, R., Mattoo, S., Munchak, L., Remer, L., Sayer, A., Patadia, F., & Hsu, N. (2013). The collection 6 MODIS aerosol products over land and ocean. *Atmospheric Measurement Techniques*, *6*(11), 2989–3034. https://doi.org/10.5194/amt-6-2989-2013

Levy, R., Remer, L., Kleidman, R., Mattoo, S., Ichoku, C., Kahn, R., & Eck, T. (2010). Global evaluation of the collection 5 MODIS dark-target aerosol products over land. *Atmospheric Chemistry and Physics*, *10*(21), 10399–10420. https://doi.org/10.5194/acp-10-10399-2010

Li, L., Che, H., Derimian, Y., Dubovik, O., Schuster, G. L., Chen, C., et al. (2020). Retrievals of fine mode light-absorbing carbonaceous aerosols from POLDER/PARASOL observations over East and South Asia. *Remote Sensing of Environment*, *247*, 111913.

Li, X., & Bourg, I. C. (2019). How secondary organic aerosol affects precipitation and radiative forcing. In *AGU Fall Meeting Abstracts* (Vol. 2019, pp. A53M–2939).

Li, X., & Bourg, I. C. (2024). Hygroscopic growth of adsorbed water films on smectite clay particles. *Environmental Science & Technology*, *58*(2), 1109–1118. https://doi.org/10.1021/acs.est.3c08253

Lopatin, A., Dubovik, O., Fuertes, D., Stenchikov, G., Lapyonok, T., Veselovskii, I., et al. (2021). Synergy processing of diverse ground-based remote sensing and in situ data using the grasp algorithm: Applications to radiometer, lidar and radiosonde observations. *Atmospheric Measurement Techniques*, *14*(3), 2575–2614. https://doi.org/10.5194/amt-14-2575-2021

O'neill, N., Eck, T., Smirnov, A., Holben, B., & Thulasiraman, S. (2003). Spectral discrimination of coarse and fine mode optical depth. *Journal of Geophysical Research*, *108*(D17), 4559. https://doi.org/10.1029/2002jd002975

O'Neill, N. T., Dubovik, O., & Eck, T. F. (2001). Modified Ångström exponent for the characterization of submicrometer aerosols. *Applied Optics*, *40*(15), 2368–2375. https://doi.org/10.1364/ao.40.002368

O'Neill, N. T., Ranjbar, K., Ivănescu, L., Eck, T. F., Reid, J. S., Giles, D. M., et al. (2023). Relationship between the sub-micron fraction (SMF) and fine-mode fraction (FMF) in the context of aeronet retrievals. *Atmospheric Measurement Techniques*, *16*(4), 1103–1120. https://doi.org/10.5194/amt-16-1103-2023

Pérez-Ramírez, D., Veselovskii, I., Whiteman, D., Suvorina, A., Korenskiy, M., Kolgotin, A., et al. (2015). High temporal resolution estimates of columnar aerosol microphysical parameters from spectrum of aerosol optical depth by linear estimation: Application to long-term AERONET and star-photometry measurements. *Atmospheric Measurement Techniques*, *8*(8), 3117–3133. https://doi.org/10.5194/amt-8-3117-2015

Pu, B., & Ginoux, P. (2016). The impact of the pacific decadal oscillation on springtime dust activity in Syria. *Atmospheric Chemistry and Physics*, *16*(21), 13431–13448. https://doi.org/10.5194/acp-16-13431-2016

Pu, B., & Ginoux, P. (2018). Climatic factors contributing to long-term variations in surface fine dust concentration in the United States. *Atmospheric Chemistry and Physics*, *18*(6), 4201–4215. https://doi.org/10.5194/acp-18-4201-2018

Pu, B., Ginoux, P., Guo, H., Hsu, N. C., Kimball, J., Marticorena, B., et al. (2020). Retrieving the global distribution of the threshold of wind erosion from satellite data and implementing it into the geophysical fluid dynamics laboratory land–atmosphere model (GFDL AM4. 0/LM4. 0). *Atmospheric Chemistry and Physics*, *20*(1), 55–81. https://doi.org/10.5194/acp-20-55-2020

Pu, B., Ginoux, P., Kapnick, S. B., & Yang, X. (2019). Seasonal prediction potential for springtime dustiness in the United States. *Geophysical Research Letters*, *46*(15), 9163–9173. https://doi.org/10.1029/2019gl083703

Pu, B., Jin, Q., Ginoux, P., & Yu, Y. (2022). Compound heat wave, drought, and dust events in California. *Journal of Climate*, *35*(24), 8133–8152. https://doi.org/10.1175/jcli-d-21-0889.1

Reid, J. S., Eck, T. F., Christopher, S. A., Hobbs, P. V., & Holben, B. (1999). Use of the Ångstrom exponent to estimate the variability of optical and physical properties of aging smoke particles in Brazil. *Journal of Geophysical Research*, *104*(D22), 27473–27489.

Sayer, A., Hsu, N., Lee, J., Bettenhausen, C., Kim, W., & Smirnov, A. (2018). Satellite ocean aerosol retrieval (SOAR) algorithm extension to S-NPP VIIRS as part of the "Deep Blue" aerosol project. *Journal of Geophysical Research: Atmospheres*, *123*(1), 380–400. https://doi.org/10.1002/2017jd027412

Sayer, A. M., Hsu, N., Bettenhausen, C., & Jeong, M.-J. (2013). Validation and uncertainty estimates for MODIS collection 6 "Deep Blue" aerosol data. *Journal of Geophysical Research: Atmospheres*, *118*(14), 7864–7872. https://doi.org/10.1002/jgrd.50600

Sayer, A. M., Hsu, N., Bettenhausen, C., Jeong, M.-J., Holben, B., & Zhang, J. (2012). Global and regional evaluation of over-land spectral aerosol optical depth retrievals from SeaWiFS. *Atmospheric Measurement Techniques*, *5*(7), 1761–1778. https://doi.org/10.5194/amt-5-1761-2012

Sayer, A. M., Hsu, N. C., Lee, J., Kim, W. V., & Dutcher, S. T. (2019). Validation, stability, and consistency of MODIS collection 6.1 and VIIRS version 1 deep blue aerosol data over land. *Journal of Geophysical Research: Atmospheres*, *124*(8), 4658–4688. https://doi.org/10.1029/2018jd029598

Schmeisser, L., Andrews, E., Ogren, J. A., Sheridan, P., Jefferson, A., Sharma, S., et al. (2017). Classifying aerosol type using in situ surface spectral aerosol optical properties. *Atmospheric Chemistry and Physics*, *17*(19), 12097–12120. https://doi.org/10.5194/acp-17-12097-2017

Sinyuk, A., Holben, B. N., Eck, T. F., Giles, D. M., Slutsker, I., Korkin, S., et al. (2020). The AERONET version 3 aerosol retrieval algorithm, associated uncertainties and comparisons to version 2. *Atmospheric Measurement Techniques*, *13*(6), 3375–3411. https://doi.org/10.5194/amt-13-3375-2020

Wagner, F., & Silva, A. (2008). Some considerations about Ångström exponent distributions. *Atmospheric Chemistry and Physics*, *8*(3), 481–489. https://doi.org/10.5194/acp-8-481-2008

Yan, X., Zang, Z., Liang, C., Luo, N., Ren, R., Cribb, M., & Li, Z. (2021). New global aerosol fine-mode fraction data over land derived from MODIS satellite retrievals. *Environmental Pollution*, *276*, 116707. https://doi.org/10.1016/j.envpol.2021.116707

Yan, X., Zang, Z., Zhao, C., & Husi, L. (2021). Understanding global changes in fine-mode aerosols during 2008–2017 using statistical methods and deep learning approach. *Environment International*, *149*, 106392. https://doi.org/10.1016/j.envint.2021.106392

Yu, Y., & Ginoux, P. (2022). Enhanced dust emission following large wildfires due to vegetation disturbance. *Nature Geoscience*, *15*(11), 878–884. https://doi.org/10.1038/s41561-022-01046-6